



Biomarker Proxy Records of Arctic Climate Change During the Mid-Pleistocene Transition from Lake El'gygytyn (Far East Russia)

Kurt R. Lindberg^{1,2}, William C. Daniels¹, Isla S. Castañeda¹, Julie Brigham-Grette¹

¹University of Massachusetts Amherst, Amherst, MA, 01003, U.S.A.

²Now at: University at Buffalo, Buffalo, NY, 14260, U.S.A.

Correspondence to: Kurt R. Lindberg (kurtlind@buffalo.edu)

Abstract. The Mid-Pleistocene Transition (MPT) is a widely recognized global climate shift occurring between approximately 1,250 to 700 ka. At this time, Earth's climate underwent a major transition from dominant 40 kyr glacial-interglacial cycles to quasi-100 kyr cycles. The cause of the MPT remains a puzzling aspect of Pleistocene climate. Presently, there are few, if any, continuous MPT records from the Arctic yet understanding the role and response of the high latitudes to the MPT is required to better evaluate the causes of this climatic shift. Here, we present new continental biomarker records of temperature and vegetation spanning 1,142 to 752 ka from Lake El'gygytyn (Far East Russia). We reconstruct warm-season temperature variations across the MPT based on branched glycerol dialkyl glycerol tetraethers (brGDGTs) using the MBT'_{5ME} proxy. The new Arctic temperature record does not display an overall cooling trend during the MPT but does exhibit strong glacial-interglacial cyclicity. Spectral analysis demonstrates persistent obliquity and precession pacing over the study interval and reveals substantial sub-orbital temperature variations at ~900 kyr during the first "skipped" interglacial. Interestingly, Marine Isotope Stage (MIS) 31, which is widely recognized as a particularly warm interglacial, does not exhibit exceptional warmth at Lake El'gygytyn. Instead, we find that MIS 29, 27 and 21 were as warm or warmer than MIS 31. In particular, MIS 21 (~870 to 820 ka) stands out as an especially warm and long interglacial in the continental Arctic while MIS 25 is a notably cold interglacial. Throughout the MPT, Lake El'gygytyn pollen data exhibits a long-term drying trend, with a shift to an increasingly open landscape noted after around 900 ka (Zhao et al., 2018), which is also reflected in our higher plant leaf wax (*n*-alkane) distributions. Although the mechanisms driving the MPT remain a matter of debate, our new climate records from the continental Arctic exhibit some similarities to changes noted around the North Pacific region. Overall, the new organic geochemical data from Lake El'gygytyn contribute to expanding our knowledge of the high-latitude response to the MPT.

1 Introduction

Since the start of the Industrial Revolution, high-latitude temperatures have increased at about twice the global average rate (Serreze et al., 2009; Davy et al., 2018). Likewise, during past interglacial periods, Arctic temperature reconstructions indicate significant warming events (e.g., de Wet et al., 2016). The importance of studying past Arctic temperature variability is widely recognized (Miller et al., 2010; Melles et al., 2012; Brigham-Grette et al., 2013) yet few long and continuous records exist from the continental Arctic. Lake El'gygytyn, located in Far East Arctic Russia, is a unique site that escaped continental glaciation and preserves a 3.6 myr-long sedimentary record (Nolan and Brigham-Grette, 2007; Melles et al., 2012). Prior work on Lake El'gygytyn has revealed exceptional changes during the Plio-Pleistocene. During the Pliocene, cool mixed forest and cool conifer forest dominated the landscape indicating a significantly warmer climate (Brigham-Grette et al., 2013) while today the lake is surrounded by tundra vegetation and tree line lies ~150 km to the southwest (Brigham-Grette et al., 2007). In addition to notable changes between Pliocene and Pleistocene climates (Brigham-Grette et al., 2013; Melles et al., 2012),



40 significant climate variability within the Pleistocene is documented at Lake El'gygytgyn (Melles et al., 2012; Wennrich et al., 2013; Francke et al., 2013), including the presence of numerous exceptionally warm "super interglacial" periods that were characterized by elevated temperature (4-5 °C warmer) and precipitation (up to 6 times higher) compared to the Holocene (Melles et al., 2012). Prior studies of Lake El'gygytgyn have also noted a signal of the Mid-Pleistocene Transition (MPT) (Melles et al., 2012; Francke et al., 2013; Wennrich et al., 2014), a globally recognized event that occurred from 1.2–0.6 Ma when variations in global ice volume shifted from exhibiting a dominant 41 kyr periodicity to a 100 kyr periodicity (Past Interglacial Working Group of PAGES, 2016).

45 The cause of the MPT remains a highly debated and puzzling aspect of Pleistocene climate. Between 900 and 650 ka glacial-interglacial cycles grew longer, more intensified, and asymmetric in association with increasingly large northern hemisphere glacial-stage ice sheets (Maslin and Ridgeway, 2005 and references therein). The MPT cannot be attributed to changes in Earth's orbital parameters (eccentricity, obliquity, precession) and thus the cause is believed to be internal to the global climate system (e.g., Berger and Loutre, 1991; Maslin and Ridgeway, 2005). Numerous, non-exclusive explanations have been proposed to explain the MPT. These include gradual removal of regolith from the northern high latitudes allowing for greater vertical growth of the northern ice sheets by increasing basal friction (Roy et al., 2004; Clark and Pollard, 1998; Willeit et al., 2019), an increase in Antarctic ice volume (Pollard and DeConto, 2009; Elderfield et al., 2012; Billups et al., 2018), and significant changes in Atlantic (Poirier and Billups, 2014), Pacific (Martínez-García et al., 2010) or Southern Ocean circulation (Hasenfratz et al., 2019; Rodríguez-Sanz et al., 2012; Pena and Goldstein, 2014). Gradual atmospheric carbon dioxide ($p\text{CO}_2$) drawdown and associated climatic cooling are also commonly cited causes of the MPT (Clark et al., 2006; Raymo, 1997; Saltzman and Verbitsky, 1993; Paillard, 1998; Hönlisch et al., 2009; Willeit et al., 2019) although empirical evidence for declining $p\text{CO}_2$ levels across the early and mid-Pleistocene remain equivocal (Da et al., 2019). As a corollary to the $p\text{CO}_2$ explanation, it has been suggested that the North Pacific and Bering Sea region may have played an important role. For example, the closure of the Bering Strait combined with expanded sea ice cover at 920 ka worked to suppress CO_2 ventilation from the subarctic North Pacific to the atmosphere (Kender et al., 2018; Worne et al., 2020). Likewise, Müller et al. (2018) propose that changes in iron fertilization to the northeast Pacific from glaciogenic Alaskan dust and ice rafting helped to drive global climate changes noted during the MPT.

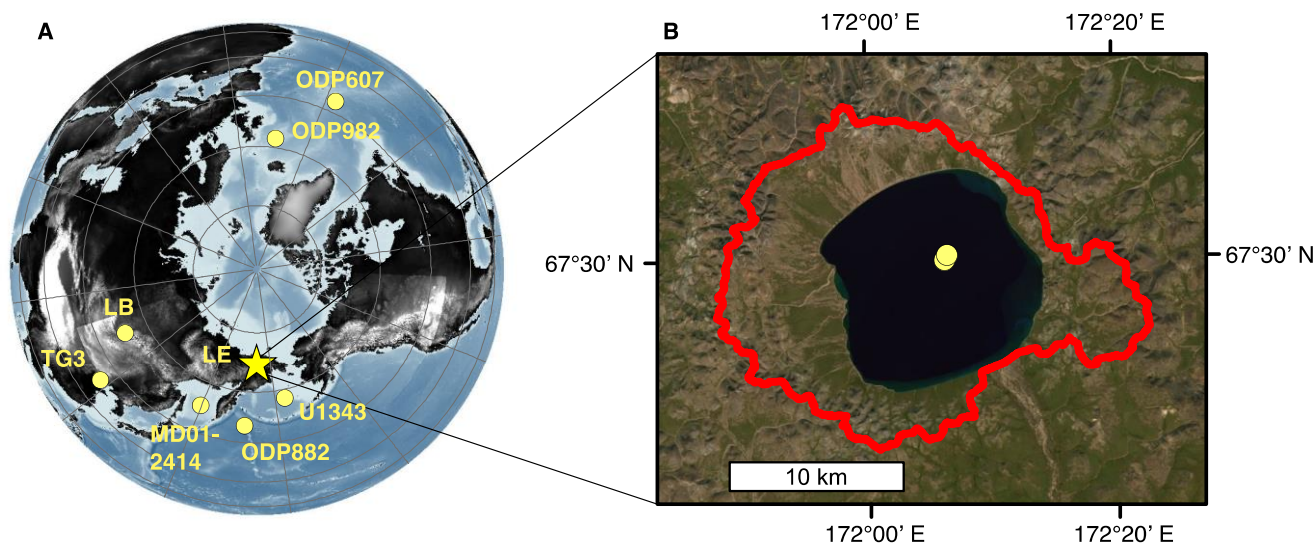
65 A complete understanding of the Arctic's role in the MPT requires continuous paleotemperature records spanning this interval. In this study, we examine the organic geochemistry of Lake El'gygytgyn sediments from 1,142 to 752 kyr to reconstruct continental arctic temperature and environmental variability during the MPT. Specifically, we use branched glycerol dialkyl tetraethers (brGDGTs; Sinninghe Damsté et al., 2000; Weijers et al., 2007), bacterial membrane lipids, to reconstruct past temperature and the distribution of long-chain n -alkanes, biomarkers of terrestrial higher plants, to examine past vegetation shifts (Bush and McInerney, 2013). While the MPT has been widely documented at globally distributed marine sites (e.g., Clark et al., 2006) and in continental loess records from Asia and Europe (Heslop et al., 2002; Han et al., 2012), lacustrine



records spanning the MPT are particularly rare. Investigating the cause(s) of the MPT is beyond the scope of this study. However, our new records provide important information regarding high-latitude continental temperature during this critical climate transition. This study also provides new insights on the strength and duration of past interglacials in the continental
75 arctic. Understanding past Arctic temperature variability is particularly important for placing the current warming into context and for improving models of future climate.

2. Study Location

Lake El'gygytyn (67.5 °N, 172.1 °E, 492 masl) is located within the Anadyr Highlands of Northeast Russia, approximately 150 km south of the Arctic Ocean coast (Fig. 1). It is a crater lake, formed following a meteorite impact at 3.58 Ma (Layer,
80 2000), that has accumulated a continuous sedimentary record since its formation. The 318 m sedimentary sequence was collected in 2009 (Melles et al., 2012; Brigham-Grette et al., 2013), providing a uniquely long Arctic paleoclimate record including the MPT interval (Melles et al., 2012; Brigham-Grette et al., 2013; Nowaczyk et al., 2013; Zhao et al., 2018). The age model for the Lake El'gygytyn drill core was previously published by Nowaczyk et al. (2013) and is applied here.



85 **Figure 1: Study location.** a) Map showing the location of Lake El'gygytyn (star) and other key sites discussed in the text (yellow
circles) including Ocean Drilling Program (ODP) Sites 882 (Martínez-García et al., 2010), 607 (Sosdian and Rosenthal, 2009), 982
(Lawrence et al., 2009) and International Ocean Discovery Program (IODP) Site U1343 (Kender et al., 2018), MD01-2414 (Lattaud
90 et al., 2018), and Tianjin-G3 loess profile (Zhou et al., 2018). B) Satellite image of Lake El'gygytyn. The yellow dot represents the
coring location of ICDP Site 5011-1 in the central lake basin and the red outline designates the lake's watershed. World imagery
sources: Esri, Maxar, GeoEye, Earthstar Geographics, CNES/Airbus DS, USDA, AeroGRID, IGN, and the GIS User Community.

The lake basin morphology and local meteorology are well-characterized by Nolan and Brigham-Grette (2007). The lake is approximately 12 km wide and 175 m deep and resides in an impact crater 18 km in width. There is a single stream outlet, the



Enmyvaam River, which drains to the south into the Bering Sea. Approximately 50 small streams, with headwaters located
95 within the impact crater, drain into the lake. Mean annual air temperature is $-10.3\text{ }^{\circ}\text{C}$ and summer temperatures average $10\text{ }^{\circ}\text{C}$.
In contrast, the lake water never exceeds $4\text{ }^{\circ}\text{C}$ except over shallower regions and in the fringing lagoons which reach $5\text{-}6\text{ }^{\circ}\text{C}$
(Nolan and Brigham-Grette, 2007). Over the past 50 years, air temperatures have risen by over $3\text{ }^{\circ}\text{C}$, driven largely by
increasing wintertime temperatures (Nolan et al., 2013). While positive air temperature anomalies are associated with a strong
low-pressure system over the Bering Sea and high pressure over the Beaufort Sea, which advects warm air from the south and
100 east, Nolan et al. (2013) demonstrated that over the observational period, the warming has resulted from thermodynamic
changes, rather than changes to the atmospheric dynamics. It is somewhat unclear if mean weather patterns at Lake
El'gygytyn are subject to reorganization over longer timescales, such as might be associated with Bering Land Bridge
exposure or submergence, or changes in North Pacific Ocean circulation.

3. Methods

105 In this study, we analyzed 127 samples from the Lake El'gygytyn drill core (ICDP Site 5011-1) spanning the interval from
1,142 ka to 752 ka, corresponding to depths of 31.06 m to 46.77 m in the composite profile. Additionally, we re-analyzed 41
samples from the study of de Wet et al. (2016), which spans Marine Isotope Stage (MIS) 33 to MIS 31 (1.11 to 1.05 Ma),
using a newer High-Performance Liquid Chromatography (HPLC) method to better separate brGDGT isomers (Hopmans et
al., 2016). We also include 85 *n*-alkane samples from the prior study by de Wet (2017) in our analysis. Overall, the sample
110 spacing averages 2.3 kyr for the brGDGTs and 2.7 kyr for the *n*-alkanes, with each 1 cm interval integrating an average 450
years, thereby allowing sufficient resolution to evaluate orbital-scale climate variability.

3.1 Biomarker Analyses

Sediment samples were freeze-dried, homogenized, and extracted using a Dionex accelerated solvent extractor (ASE 200) with
a mixture of 9:1 of dichloromethane: methanol (v/v). Known quantities of a synthetic C_{46} GDGT were added to the total lipid
115 extract (TLE) as an internal standard (Huguet et al., 2006). The TLE was then separated via alumina oxide columns using 9:1
hexane: dichloromethane (v/v) to elute the apolar fraction and 1:1 dichloromethane: methanol (v/v) to elute the polar fraction.

3.1.1 *n*-alkane analysis

Apolar fractions were analyzed on an Agilent 7890A gas chromatograph-flame ionization detector (GC-FID) to determine
concentrations of the *n*-alkanes. Samples were run in splitless mode with an inlet temperature of $250\text{ }^{\circ}\text{C}$ and inlet flow rate of
120 26.5 mL min^{-1} , using hydrogen as the carrier gas. Separation was achieved using a 5% phenyl methyl siloxane column (HP-5;
 $60\text{ m} \times 320\text{ }\mu\text{m} \times 0.25\text{ }\mu\text{m}$), with a flow rate of 4.6 mL min^{-1} . The oven temperature program was as follows: $70\text{ }^{\circ}\text{C}$ for two
minutes, increasing at $17\text{ }^{\circ}\text{C min}^{-1}$ to $130\text{ }^{\circ}\text{C}$, then increasing at $7\text{ }^{\circ}\text{C min}^{-1}$ to $320\text{ }^{\circ}\text{C}$, and finally holding at $320\text{ }^{\circ}\text{C}$ for 15
minutes. Compound identification was performed by comparison to a standard mixture of $\text{C}_{21}\text{-C}_{40}$ *n*-alkanes injected during



each run and by confirming compound identification for a subset of samples via GC-mass spectrometry, following the methods
125 detailed in Keisling et al. (2017). Concentrations of each *n*-alkane were determined using an external squalene calibration
curve. Here, we examine leaf wax distributions using the Average Chain Length (ACL; Bray and Evans, 1961; Bush and
McInerney, 2013), calculated for the terrestrial (C₂₇ to C₃₃) *n*-alkanes (Eq. 1):

$$(1) \text{ACL} = \frac{\sum(C_n * n)}{\sum(C_n)}$$

3.1.2 GDGT analysis

130 The polar fractions were filtered through a 0.45 µm PTFE filter in 99:1 hexane: isopropanol (v/v). Isoprenoid glycerol dialkyl
glycerol tetraethers (iGDGTs) and brGDGTs were analyzed using an Agilent 1260 Ultra High-Performance Liquid
Chromatograph (UHPLC) coupled to an Agilent 6120 single quadrupole mass selective detector (MSD) and following the
methods detailed by Hopmans et al. (2016), which separates the 5- and 6-methyl brGDGT isomers. Briefly, separation is
135 achieved using a silica precolumn with two BEH HILIC columns in series (2.1 x 150 mm, 1.7 µm; Waters®). Samples were
eluted using hexane (solvent A) and hexane:isopropanol (9:1 v/v; solvent B) in the following program: 18% solvent B for 25
minutes, a linear increase to solvent B over 25 minutes, then a linear increase to 100% solvent B for 30 minutes. The column
temperature was 30°C and the flow rate was 0.2 ml min⁻¹. Compounds were ionized using atmospheric pressure chemical
ionization and the MSD was run in single ion monitoring (SIM) mode for the GDGT core lipids.

140 Lake El'gygytgyn sediments are dominated by brGDGTs with only small concentrations of iGDGTs present (Holland et al.,
2013; D'Anjou et al., 2013; de Wet et al., 2016; Keisling et al., 2017; Daniels et al., in review). Thus, we use the Methylation
of Branched Tetraethers index (eq. 2), considering only the 5-methyl isomers (MBT'_{5ME}), to reconstruct past temperature (De
Jonge et al., 2014).

$$(2) \text{MBT}'_{5\text{ME}} = \frac{[\text{Ia} + \text{Ib} + \text{Ic}]}{[\text{Ia} + \text{Ib} + \text{Ic}] + [\text{IIa} + \text{IIb} + \text{IIc}] + [\text{IIIa} + \text{IIIb} + \text{IIIc}]}$$

145 We explore the use of several lacustrine brGDGT calibrations to convert MBT'_{5ME} values to temperature. The first is based on
a suite of lakes in East Africa that span an elevation transect to capture temperature gradients (Russell et al., 2018; eq. 3). This
calibration is to mean annual air temperature.

$$(3) \text{MAAT} = -1.21 + 32.42 * \text{MBT}'_{5\text{ME}} \quad (\text{RMSE} = 2.44 \text{ } ^\circ\text{C})$$

More recently, Zhao et al. (2021) developed an in-situ calibration to summer (JJA) water temperature using sediment trap data
150 from a site in southern Greenland (eq. 4).

$$(4) \text{JJA Water Temp} = -1.82 + 56.06 * \text{MBT}'_{5\text{ME}} \quad (\text{RMSE} = 0.58 \text{ } ^\circ\text{C})$$

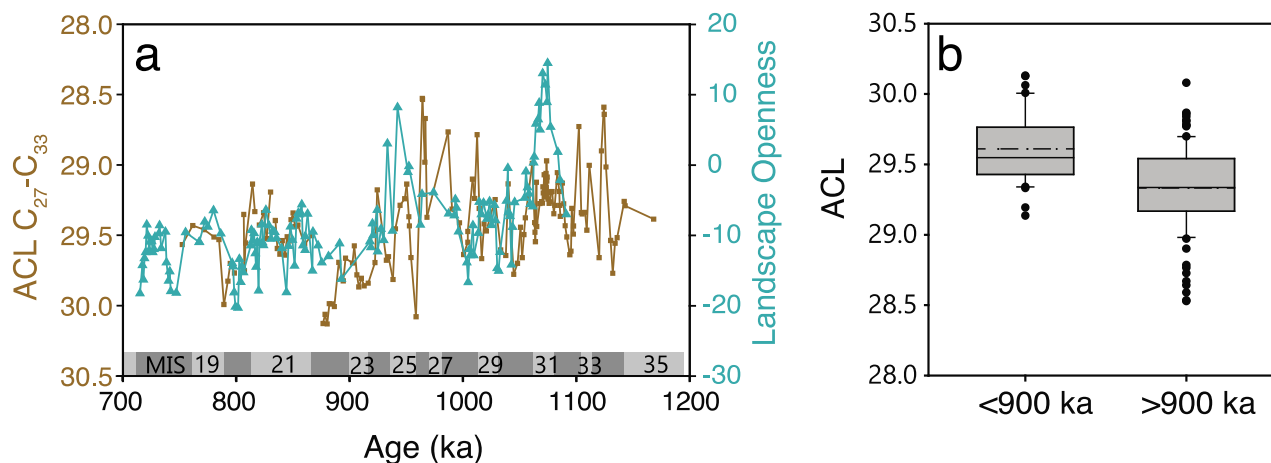
We also apply the global Bayesian calibration for lacustrine brGDGTs, known as BayMBT, using the baymbt_predict()
MATLAB function (Martinez-Sosa et al., 2021). Following the approach of Martinez-Sosa et al. (2021), we estimated the prior
value for our dataset by calculating a mean temperature using the Russell et al. (2018) calibration; we also used 10°C for the
155 standard deviation.



4. Results

4.1 *n*-alkanes

Plant leaf waxes (*n*-alkanes) were present in all samples. However, 58 of the 211 samples analyzed (27%) contained an unresolved complex mixture in the apolar fractions, hampering peak identification without further sample purification. The *n*-alkanes were not quantified for these samples, resulting in lower sample resolution record for the leaf waxes compared to the GDGTs. For the 153 samples where they could be sufficiently resolved, samples contained C₂₀ through C₃₃ *n*-alkanes, with the shorter chain lengths not always present in each sample. The total concentration of odd-numbered *n*-alkanes ranges from 0.6 to 60.8 μg g⁻¹, with a mean concentration of 4.5 μg g⁻¹. Odd-numbered chain lengths dominate, particularly the C₂₃ and C₂₇ homologues (Fig. S1), and the carbon preference index (CPI) over the C₂₅-C₃₃ compounds averages 3.6 (±0.6 s.d.). When considering all *n*-alkanes from C₁₇ to C₃₃, the ACL averages 26.2 (±0.9 s.d.). The C₂₇-C₃₃ ACL (Eq. 1) varied between 28.5 and 30.1 (Fig. 2a), with a mean of 29.4. The C₂₇-C₃₃ ACL exhibits a clear shift at around 900 ka; samples older than 900 ka samples characterized by lower ACL values whereas samples younger than 900 ka exhibit higher ACL values (Fig. 2b).



170 **Figure 2: Comparison of Lake El'gygytgyn *n*-alkane and pollen data. A) The ACL of the C₂₇-C₃₃ *n*-alkanes (brown squares) plotted along with the Landscape Openness Index derived from pollen spectra (teal triangles; data from Zhao et al. (2018)). B) Boxplots of the ACL data for all samples younger than 900 ka and all samples older than 900 ka. The solid line represents the median value and the dashed line the mean. Individual outliers are plotted.**

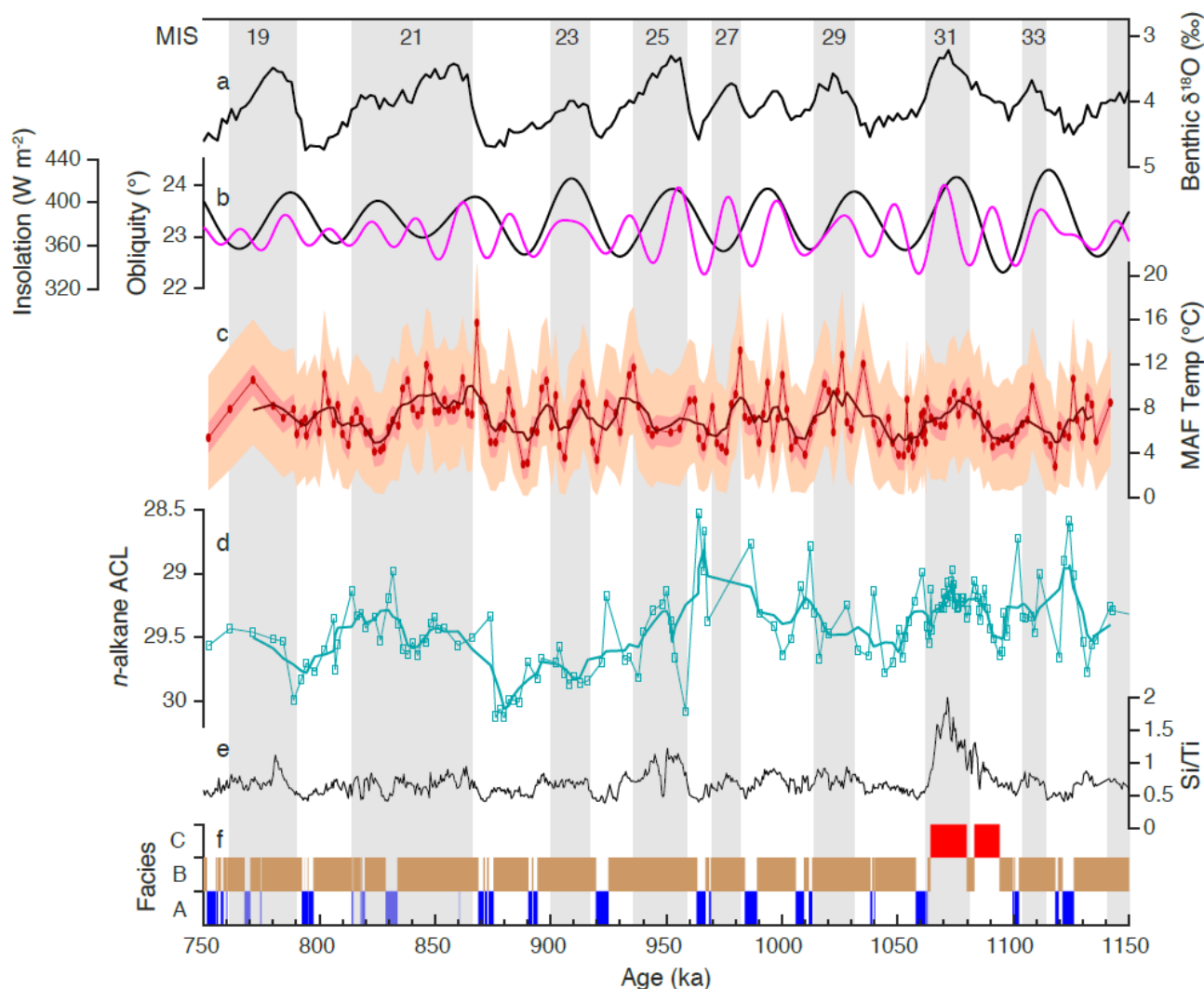
4.2 GDGTs

175 iGDGTs are present in all samples analyzed. However, total iGDGT concentrations are low and range from 0.3 ng g⁻¹ to 3916 ng g⁻¹ with a mean concentration of 69 ng g sed⁻¹ (Fig. S2). Nearly all the iGDGTs present are represented by GDGT-0 and GDGT-4 (Daniels et al., in review), with average abundances of 75% and 15% of the total iGDGTs. The high



GDGT0/crenarchaeol ratio (average 68.8), as well as the fact that many samples did not contain all of the iGDGTs required to calculate a TEX₈₆ value, precludes the use of the TEX₈₆ paleothermometer (Schouten et al., 2002) at Lake El'gygytyn. This result is consistent with prior investigations of different time intervals of the Lake El'gygytyn record (D'Anjou et al., 2013; Holland et al., 2013; de Wet et al., 2016; Keisling et al., 2017; Daniels et al., in review).

Within the entire 174 sample dataset, including the re-analyzed samples from de Wet et al. (2016), total brGDGT concentrations vary from 15 to 4561 ng g sed⁻¹ with a mean concentration of 237 ng g sed⁻¹ (Fig. S2). Like other Arctic lake sediment records (Zhao et al., 2021; Thomas et al., 2018; Raberg et al., 2021; Peterse et al., 2014) hexamethyl brGDGTs (IIIa, IIIb, IIIc) dominate the brGDGT assemblages (46%), followed by pentamethyl brGDGTs (IIa, IIb, IIc, 30%), then tetramethyl brGDGTs (Ia, Ib, Ic, 23%) (Fig. S2). We observe 6-methyl GDGT isomers in all samples, which comprise an average of 9% of the total brGDGTs present but can be as high as 33% and exhibit substantial variability (Fig. S3). MBT'_{SME} values range from 0.12 to 0.56 with an average of 0.28. Based on triplicate analysis of 12 samples, the analytical uncertainty (1σ) of the MBT'_{SME} is 0.0065. Typically, glacial-interglacial changes in MBT'_{SME} are on the order of 0.1 to 0.15 units, equivalent to 5-8°C on the Greenland lakes calibration (Zhao et al., 2021) and ca. 3-5°C on both the African lakes (Russell et al., 2018) and BayMBT (Martinez-Sosa et al., 2021) calibrations (Fig. S4). The BayMBT temperature reconstruction of months above freezing is shown in Fig. 3.



195 **Figure 3: Lake El'gygytyn data.** The marine isotope stages are indicated at the top of the diagram. A) global composite benthic foraminifera oxygen isotopes (Lisiecki and Raymo, 2005). B) Astronomical forcing, including obliquity (magenta) and summer insolation (June 21-Sept 21) at 65 °N latitude (Laskar et al., 2004). C) brGDGT-inferred temperature of the months above freezing (MAF Temp). Dark shading represents the 1 σ analytical uncertainty based on triplicate MBT'_{SME} analyses converted to temperature using BayMBT (1 σ =1.35 °C, n=12), while light shading represents the calibration uncertainty of the BayMBT application. Dark line shows the 5-point moving average. D) *n*-alkane ACL for the C₂₇-C₃₃. E) Lake El'gygytyn silica Melles et al., 2012; Wennrich et al., 2013); F) Occurrence of Melles et al., 2012). Facies A (blue bars) represents glacial intervals. Facies B (brown bars) is cosmopolitan, occurring during both glacials and interglacials. Facies C (red bars) represents superinterglacials.

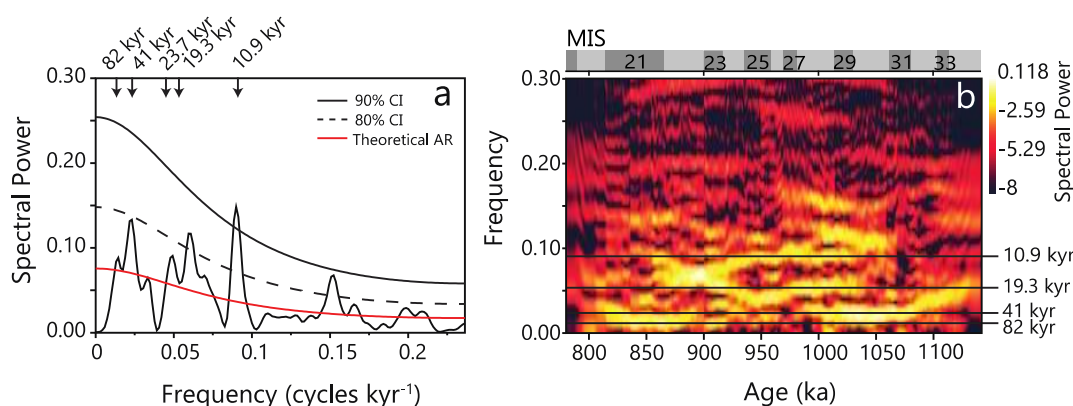
200

4.3 Spectral Signatures of Temperature Variability

205 To characterize the frequency of temperature variability, we analyzed spectral signatures of the MBT'_{SME} temperature record using PAST3 software (Hammer et al., 2001). Frequency analysis was not performed on the *n*-alkane data because of its lower



sample resolution. The REDFIT package, which utilizes the Lomb-Scargle method (Lomb, 1976; Scargle, 1982; Schulz and Mudelsee, 2002) for spectral analysis is used to evaluate the overall periodogram, while the Short-time Fourier transform package was used to generate the evolutionary periodogram. Over our study interval, the REDFIT periodogram shows a small spectral peak at ~82 kyr/cycle, a peak at ~41 kyr/cycles, a dispersed peak in the 23-14 kyr/cycle, as well as a significant peak at ~11 kyr/cycle possibly reflecting half-precession (Fig. 4a). The 40 kyr obliquity signal is strongest in the earlier part of the temperature record, from MIS 32 to MIS 26, but weakens by ~980 ka, when the relative power of the higher-frequency bands increases (Fig. 4b). Toward the later part of the record, beginning at ~900 ka, we observe increased variability at longer wavelengths, potentially reflecting both 40- and 80-kyr cyclicity (e.g., obliquity and 2x obliquity) in the temperature record.



215

Figure 4: Frequency analysis of Lake El'gygytyn MBT_{SME} data from 1142 to 752 ka. A) Lomb-Scargle periodogram, with the 80% and 90% confidence levels as well as the theoretical autoregression levels. B) Short-time Fourier transformation showing the evolutionary power spectrum, with the dominant peaks from (A) indicated with horizontal lines. Marine Isotope Stages (MIS) are indicated along the top. Both analyses were performed using PAST3 (Hammer et al., 2001).

220 5. Discussion

5.1 Interpretation of the *n*-alkane ACL record

The long-chain *n*-alkanes (*n*-alkanoic acids, *n*-alcohols) with 27 to 35 carbon atoms are biomarkers of terrestrial higher plants (Eglinton and Hamilton, 1967). Indeed, long-chain (C₂₇-C₃₃) *n*-alkanes are predominantly derived from higher terrestrial plants in the El'gygytyn catchment (Wilkie et al., 2013), similar to observations at other Arctic locations (Daniels et al., 2017; O'Connor et al., 2020). Over the MPT study interval, CPI values average 3.6 indicating that higher plant inputs dominate the *n*-alkane pool. Both the distributions and isotopic composition of *n*-alkanes can provide information on past vegetation change or the response of vegetation to climate (e.g., temperature or precipitation; Meyers, 2003; Castañeda and Schouten, 2011). We did not examine leaf wax deuterium or carbon isotopes in this study, but we observe changes in the *n*-alkane ACL across the MPT (Fig. 2). Prior studies have found ACL to increase with increasing aridity (e.g., Liu and Huang, 2005; Schefuß et al., 2003; Peltzer, 1989; Poynter et al., 1989) or increasing temperature (e.g., Castañeda et al., 2009; Zhang et al., 2006; Kawamura

230



et al., 2003; Rommerskirchen et al., 2003; Gagosian and Peltzer, 1986). However, at some locations there is no clear relationship between temperature or aridity and ACL. Furthermore, global correlations are weak hindering a quantitative climate assessment using ACL (Bush and McInerney, 2015). Nonetheless, in the Arctic, higher ACL values have been associated with arid conditions (Andersson et al., 2011). At Lake El'gygytgyn, Keisling et al. (2017) suggested that ACL
235 during the Pliocene is correlated with independent metrics of aridity but is secondarily affected by temperature and vegetation change. As there are available pollen assemblage data from Lake El'gygytgyn spanning the MPT (Zhao et al., 2018), we refine our interpretation of ACL here.

Zhao et al. (2018) examined pollen assemblages in the Lake El'gygytgyn drill core spanning 1,091 to 715 ka and found that
240 shrub tundra and cold steppe communities dominate throughout the study interval. The pollen record exhibits a clear response to glacial-interglacial climate forcing with higher percentages of herbaceous taxa (*Poaceae*, *Cyperaceae*, and *Artemisia*) present during glacial periods, reflecting an open landscape (treeless or shrubless) and cold and arid conditions. Conversely, during interglacials increased percentages of tree and shrub pollen are present, with dwarf birch (*Betula*) and shrub alder (*Alnus*) being the most common (Zhao et al., 2018). The authors developed a landscape openness index, which is the relative
245 difference between the maximum scores of forest and open biomes, as a qualitative assessment of forest vs. an open landscape (Zhao et al., 2018). This record shows higher (positive) values during interglacials, with especially high values noted during MIS 31 and MIS 25 (Fig. 2a). Throughout the MPT, a shift in the landscape openness index is observed with an increasingly open landscape noted after around 890 ka, reflecting a long-term cooling and drying trend during the MPT (Zhao et al., 2018). We find that the ACL at Lake El'gygytgyn tracks changes in the landscape openness index, with lower values observed prior
250 to ~900 ka and higher values afterwards when the landscape is more open and herbaceous taxa are more prevalent (Fig. 2b). Thus, we interpret ACL variations as representing large-scale vegetation changes around Lake El'gygytgyn, which likely reflect a combination of climate-driven vegetation change coupled with the direct response of plants to moisture availability.

5.2 Interpretation of the brGDGT record

Prior to interpreting the brGDGT record, the source(s) of the brGDGTs (soil or lacustrine), the seasonality of production, and
255 the choice of temperature calibration need to be considered. The distribution of brGDGTs in our dataset indicates a dominant lacustrine source (Fig. S5) throughout the MPT, in agreement with other previously studied time intervals of the Lake El'gygytgyn record (Holland et al., 2013; D'Anjou et al., 2013; de Wet et al., 2016; Keisling et al., 2017). Moreover, the samples are dominated by 5-methyl brGDGTs, suggesting that the MBT'_{5ME} index is most suitable for reconstructing temperatures at Lake El'gygytgyn (Fig. S2, S3). There are currently several lacustrine MBT'_{5ME} calibrations that can be applied
260 to reconstruct past temperature (Dang et al., 2018; Russell et al., 2018; Zhao et al., 2020; Martinez-Sosa et al., 2021). The calibration of Dang et al. (2018) is based on alkaline lakes, and so is inappropriate to apply at Lake El'gygytgyn, which has a pH of ~6 (Cremer et al., 2005). The calibration of Russell et al. (2018) reconstructs mean annual air temperature and is based on a suite of tropical African lakes while the Zhao et al. (2021) calibration reconstructs summer water temperature and is based

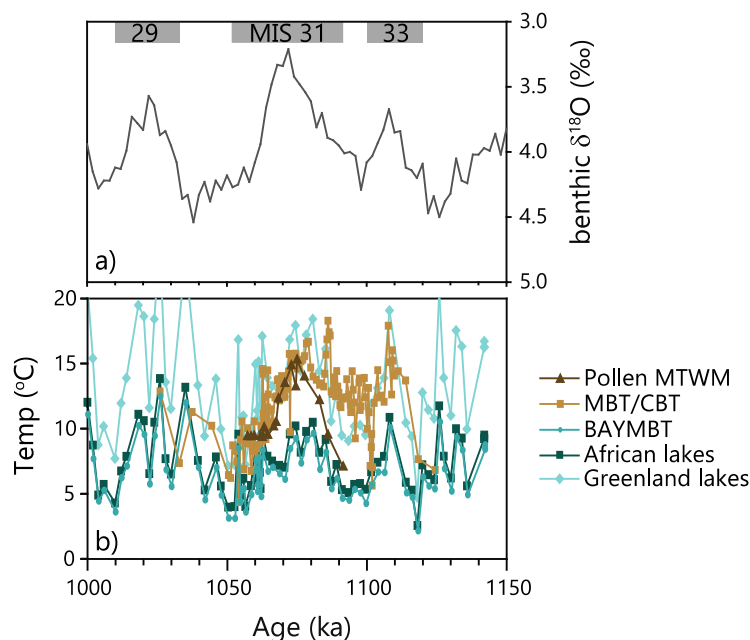


265 on settling particulate material from a southern Greenland lake. The global Bayesian calibration includes globally distributed lakes, although there are few Arctic sites outside of Alaska (Martinez-Sosa et al., 2021). It should be noted that the Zhao et al. (2021) calibration is currently the only MBT'_{SME} calibration to water temperature; the other studies calibrate to mean annual air temperature or air temperature of months above freezing because in-situ measurements of lake water temperature are often not available.

270 All lacustrine brGDGT calibrations yield similar downcore patterns but the magnitude of temperature variability as well as the absolute values varies between calibrations (Fig. S4). Reconstructed temperatures using the African lakes calibration (Russell et al., 2018) range from 2.2 to 17.0 °C, with a mean of 7.8 °C. Temperatures based on the Greenland calibration (Zhao et al., 2021) range from 4.0 to 29.7 °C, with a mean of 13.6 °C. The lacustrine BayMBT calibration (Martinez-Sosa et al., 2021) yields median values ranging from 2.8 to 15.7 °C, with an average of 7.1 °C.

275

For MIS 31 (1.082–1.062 Ma), which is widely recognized as an exceptionally warm interglacial period (e.g., Maiorano et al., 2009; Teitler et al., 2015), there are independent temperature estimates (mean temperature of the warmest month) for Lake El'gygytgyn based on pollen assemblages (Fig. 5; Melles et al., 2012). While the Greenland lakes calibration (Zhao et al., 2021) yields similar temperature estimates to the pollen-based reconstruction across MIS 31 (Melles et al., 2012; de Wet et al., 280 2016), the overall amplitude through the remainder of the study interval appears unreasonably large and thus we opt against using this calibration. Both the African lakes (Russell et al., 2018) and global Bayesian calibrations (Martinez-Sosa et al., 2021) produce similar values and yield comparatively lower MIS 31 temperatures compared to the pollen estimates, as well as an overall amplitude of temperature variability that is more realistic (Fig. 5). Therefore, throughout the remainder of this discussion we plot our MBT'_{SME} data using the BayMBT calibration (Martinez-Sosa et al., 2021). While a lacustrine-based 285 brGDGT temperature calibration needs to be applied to Lake El'gygytgyn, it should be noted that our samples display a somewhat different brGDGT distribution compared to other lake datasets (Fig. S5), potentially reflecting a need for a pan-Arctic brGDGT calibration or a site-specific calibration. We therefore place more emphasis on relative trends in the data (warming and cooling events), which remain robust regardless of the calibration applied. Furthermore, given that several studies now document that brGDGT production in high-latitude lakes peaks during summer, and that both older brGDGT 290 calibrations, which were based on combined methylation and cyclization of brGDGTs, as well as the newer MBT'_{SME} index show the strongest correlation with growing-season temperatures (Pearson et al., 2011; Sun et al., 2011; Shanahan et al., 2013; Zhao et al., 2021; Miller et al., 2018; Martinez-Sosa et al., 2021), we interpret relative temperature changes at Lake El'gygytgyn as reflecting conditions during the ice-free summer growing season.



295 **Figure 5: Comparison of brGDGT calibration during MIS 31 with pollen-derived temperature estimates (Melles et al., 2012). A)**
The global benthic oxygen isotope stack (Lisiecki and Raymo, 2005) with the different marine isotope stages (MIS) is indicated at
the top for reference. **B) Lake El'gygytyn brGDGT temperature estimates using the calibrations of Zhao et al. (2018) based on**
Greenland lakes (light blue diamonds), the African lakes MBT_{5ME} calibration of Russell et al. (2018) indicated by the dark green
squares, the MBT/CBT calibration of Sun et al. (2011) indicated by the light brown squares, this is the previously published dataset
300 from de Wet et al. (2016), the BayMBT calibration indicated by the light green circles (Martinez-Sosa et al., 2021) and pollen mean
temperature of the warmest month (MTWM) from Melles et al. (2012) indicated by the brown triangles. Note how the BayMBT and
African lakes calibrations yield similar results and nearly plot on top of each other.

5.3 Climate variability during the MPT

305 Our new brGDGT data from Lake El'gygytyn document relative temperature changes, revealing several important aspects of
orbital and long-term climate variability throughout the MPT. The MBT_{5ME} record shows that temperatures varied at
Milankovitch and sub-Milankovitch time scales, and generally follows changes noted in the global benthic oxygen isotope
stack (Lisiecki and Raymo, 2005) and insolation (Fig. 3). This observation agrees with prior studies of Lake El'gygytyn (e.g.,
de Wet et al., 2016), although it is evident that the relative importance of obliquity and precession-pacing has varied temporally
310 (Fig. 3 and 4). Our MBT_{5ME} temperature record supports the observation of Melles et al. (2012) that congruency between peak
precession, obliquity, and eccentricity, together with inter-hemispheric teleconnections can generate superinterglacial periods
such as MIS 11 and 31. The brGDGT data generally support this interpretation during MIS 31, and during the alignment of
northern hemisphere summer perihelion and obliquity during the warm MIS 21 (Huybers and Wunsch, 2005), but we note that
several other intervals are as warm in the MBT_{5ME} record despite differences in the orbital configurations. Furthermore, we



315 note that the inverse is also true for temperatures at Lake El'gygytgyn whereby congruent minima in summer insolation, obliquity, and relatively low eccentricity resulted in very cold conditions during MIS 28 and MIS 22 (Fig. 3).

We observe no long-term trend in the MBT'_{5ME} data (Fig. 3), which contrasts with cooling trends observed in the global benthic $\delta^{18}\text{O}$ stack (Lisiecki and Raymo, 2005; Clark et al., 2006; Li et al., 2004), Mg/Ca-derived temperatures of Atlantic deep waters (Sosdian and Rosenthal, 2009), and some sea surface temperature records from the northern high latitudes (e.g. Martínez-García et al., 2010; Lawrence et al., 2009; McClymont et al., 2008). This lack of MPT cooling at El'gygytgyn is difficult to explain given the expansion of northern hemisphere ice sheets at that time. It could imply that the climate at the study site is not representative of the pan-Arctic region, and indeed, there is considerable spatial variability in climate change across the Arctic. Alternatively, it may suggest that Arctic cooling was not the critical driver of intensified ice sheet growth, implicating a strong role for the regolith removal hypothesis (Clark and Pollard, 1998) or southern hemisphere (i.e. Antarctic) cooling and ice sheet expansion (Ford and Raymo, 2020). Although we see no overall trend in the brGDGT data, there is a notable increase in leaf wax ACL values reflecting a significant climate-driven ecological change across the MPT (Fig. 2), most likely indicating aridification of the study region. A long-term aridification trend over the past ~1 myr is similarly noted from the Chinese Loess Plateau (Zhao et al., 2018; Zhou et al., 2018; Wu et al., 2020). At El'gygytgyn, aridity is in part controlled by the amount of moisture being sourced from the nearby high-latitude seas. A sedimentary record from the Northwind Ridge in the Western Arctic Ocean indicates a transition from seasonal sea ice to perennial sea ice around 1 million years ago, which could explain the observed trend toward drier conditions (Dipre et al., 2018). The contrast between enhanced sea ice coverage and stable temperatures at El'gygytgyn points to strong geographic variations in climatic cooling across the MPT, particularly between the marine realm and NE Russia.

335 A characteristic feature of the MPT is the appearance of longer glacial cycles, expressed in the frequency domain of many palaeoceanographic and continental records as increasing power in the quasi-100 kyr band, although there is no fundamental change in orbital forcing across the MPT. In the Arctic, precession and obliquity are key drivers of temperatures because of the large changes in peak summer insolation and changes in summer duration. Indeed, spectral analysis of the Lake El'gygytgyn MBT'_{5ME} record reveals significant obliquity and precession cycles over the MPT (Fig. 4), with the obliquity signal being the strongest prior to ~1.0 Ma (Fig. 4). Increased variability at longer wavelengths is observed after ~900 ka but at an ~82 kyr cyclicity, which may be twice an obliquity signal rather than eccentricity. However, we note that the interval studied here may be too short to fully evaluate changes in longer orbital frequencies occurring during the MPT. Prior studies of the Lake El'gygytgyn drill core report similar spectral results but with some notable differences in the relative strength of various frequencies. Grain-size data, reflecting climate-dependent (glacial-interglacial) clastic sedimentation processes at Lake El'gygytgyn, also display a strong obliquity cycle throughout the MPT. Yet in contrast to the brGDGT data, the strongest obliquity signature is noted in the younger part of the record from 950 to 670 ka (Francke et al., 2013). The grain-size data also exhibits a strong precession cycle from 1100 to 900 ka (Francke et al., 2013), in agreement with the brGDGT data. The



350 authors note that changes in grain-size at Lake El'gygytgyn are not directly coupled to changes in global ice volume. The effect
of MPT ice sheet expansion on spectral signatures would naturally be strongest in direct proximity to where the ice sheets
develop, namely North America, Greenland, and Fenno-Scandia. In northeast Siberia, however, ice sheets have not been as
prominent a feature of the Pleistocene environment (Brigham-Grette et al., 2013), and it is not entirely clear how the 100 kyr
ice sheet influence is transferred to Lake El'gygytgyn. Through model simulations, Melles et al. (2012) indicated that
temperature variability at Lake El'gygytgyn is decoupled from Greenland Ice Sheet growth/decay. Instead, precession
355 variations here are more likely connected with regional insolation differences or latitudinal climatic teleconnections (Francke
et al., 2013), which may help explain the lack of brGDGT-inferred cooling across the MPT.

Interestingly, the Lake El'gygytgyn brGDGT data exhibit the strongest spectral power at ~10.9-kyr cyclicity (Fig. 4), which
could reflect a half-precession signal (Verschuren et al., 2009). The signal is strongest between 850 and 1030 ka, and is
360 apparent, for example, in the structure of the substages of MIS 21. Climate variations at this time scale have not been previously
reported at Lake El'gygytgyn, as most proxies are dominated by the Milankovitch frequencies. Nonetheless, half-precession
has been observed during the MPT in the northern high latitudes. Haneda et al. (2020, EPSL) report half-precession variability
in the Kuroshio current of the western North Pacific during MIS 19. Likewise, Ferretti et al. (2010) report that during MIS 21,
foraminifera $\delta^{18}\text{O}$ varied strongly at the 10.6 kyr wavelength at Site U1313 (Figure 1; this Site is a revisit of DSDP 607) and
365 a number of other sites across the North Atlantic. Their finding supports a previous identification of Milankovitch harmonics
in the North Atlantic (Wara et al., 2002). In that region, the isotope signal was driven by variations in temperature and the
strength of Atlantic Meridional Overturning Circulation (AMOC). While there are some differences in phasing among the
North Atlantic sites and compared to the Lake El'gygytgyn MBT'_{5ME}, we note that the half-precession signal is strongest at
El'gygytgyn leading up to and during MIS 21, suggesting the variations in the North Atlantic and at El'gygytgyn might be
370 linked.

The presence of half-precession variability in the North Atlantic has been attributed to non-linear feedbacks due to orbital
forcing within the North Atlantic region, related to the different timescales of ice sheet dynamics, deep ocean convection, and
moisture feedbacks (Wara et al., 2002). It has alternatively been linked to tropical hemi-precession (e.g. Verschuren et al.,
375 2009) being transmitted to the high latitudes via oceanic and atmospheric teleconnections (Ferretti et al., 2010). In the
Northwest Pacific, Haneda et al. (2020) suggest a combination of AMOC variation and equatorial insolation forcing generated
the half-precession signal there, while Thomas et al. (2016) have suggested that dynamics of ice sheets and greenhouse gasses
contribute to half-precession in monsoon regions of China during the late Pleistocene (post-MPT). At Lake El'gygytgyn, it is
difficult to determine if the ~11 kyr variability is linked to monsoon dynamics, as half-precession has not been reported for the
380 MPT from continental sites in Asia. Given that AMOC variations impact temperatures across the Arctic, we speculate that the
half-precession observed at El'gygytgyn may have been driven by changes reported by Ferretti et al. (2010) and Wara et al.



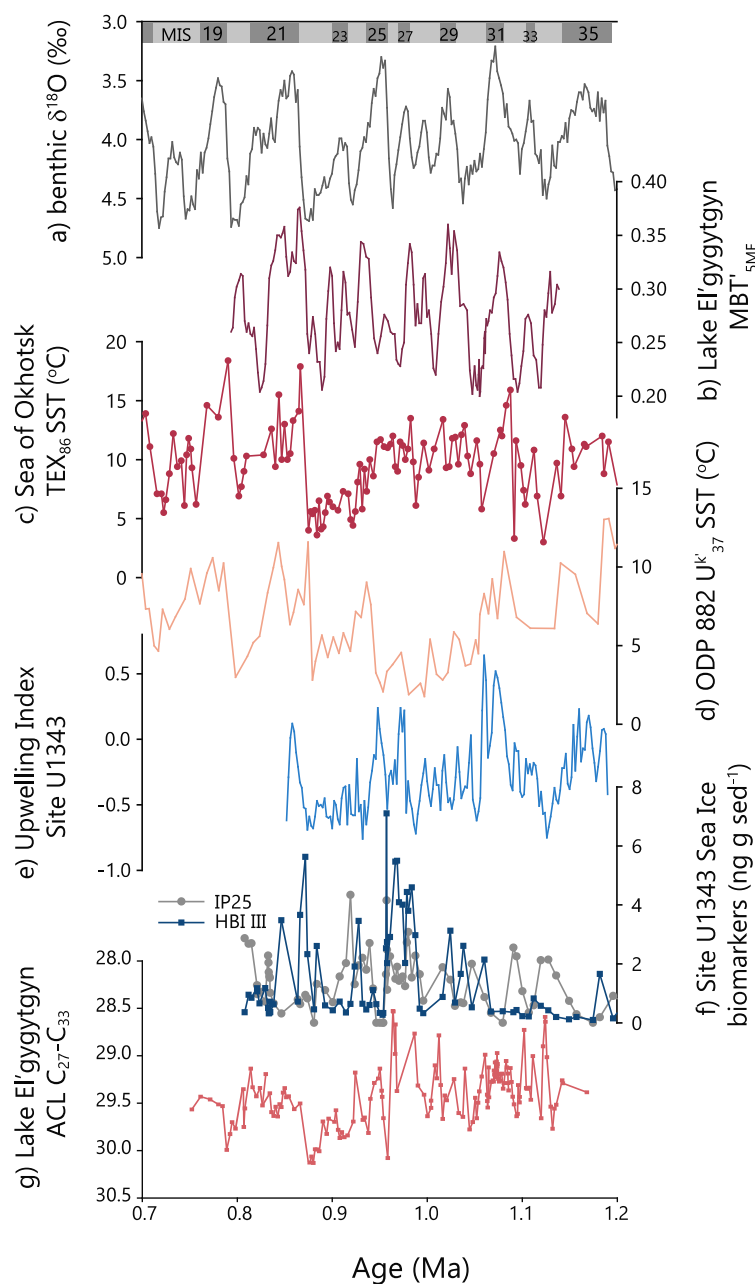
(2002). Future studies are needed to determine if the Arctic temperature is indeed reflecting a half-precession signal, and how such a signal might change in response to ice sheet and greenhouse gas conditions.

385 In the following discussion, we take a closer look at glacial-interglacial variability noted in our new Lake El'gygytgyn biomarker records.

5.3.1 MIS 34-26 (1150 to 959 ka)

In the interval spanning MIS 34 to 26, we observe a strong correspondence between the MBT'_{5ME} temperatures and global benthic foraminifera oxygen isotope ($\delta^{18}O$) stack (Lisiecki and Raymo, 2005) (Fig. 3). The coldest periods in the MBT'_{5ME} record align closely with glacial Facies A in the El'gygytgyn sediment profile (Fig. 3), as well as with biomarker inferred expansions of sea ice beyond the marginal ice zone of the Bering Sea (Fig. 6; Detlef et al., 2018) indicating cooling across the Bering region during the MIS 32, 30, 28, and 26. While precession and half-precession are apparent in the evolutionary power spectrum (Fig. 4), the temperature was primarily paced at 41 kyr over this interval, as seen in alignment between the smoothed brGDGT temperature record and the obliquity history (Fig. S6). This could reflect the importance of summer duration on Arctic summer temperature or lake water temperature. Alternatively, the 41-kyr pacing may be driven by changes in glacial/interglacial pCO_2 variations, for which there is not a well-resolved record over this timespan but it likely tracked global climate conditions at 41 kyr pacing (Berends et al., 2021).

390
395



400 **Figure 6: Comparison of the Lake El'gygytgyn temperature reconstruction across the MPT with marine records from the sub-Arctic North Pacific. A) global benthic oxygen isotope stack (Lisiecki and Raymo, 2005). B) Smoothed (5-point moving average) Lake El'gygytgyn MBT'₅ME values. C) SST from the Sea of Okhotsk (Site MD01-2414; Lattaud et al., 2018). D) SST from the sub-Arctic North Pacific (ODP 882; Martínez-García et al., 2010). E) Upwelling index in the Bering Sea (Site U1343; Worne et al., 2020). F) Concentration of sea ice biomarkers in the Bering Sea (Site U1343; Detlef et al., 2018). G. Lake El'gygytgyn leaf wax ACL values.**



During MIS 31, the MBT'_{5ME} record shows somewhat surprising results in comparison to other Lake El'gygytyn proxies (Fig. 3). In the El'gygytyn record, superinterglacial periods (interglacials that are exceptionally warm and wet) were previously identified based on the presence of Facies C, a sedimentary unit characterized by weakly laminated reddish oxidized sediments, high Si/Ti ratios, and low organic matter content (Melles et al., 2012). Facies C is interpreted as reflecting an oxygenated water column, high aquatic productivity, seasonal lake ice, and generally warm conditions (Melles et al., 2012). Pollen spectra from Facies C intervals typically corroborate this interpretation, exhibiting a temporary appearance of birch, alder or other trees (Melles et al., 2012). The MBT'_{5ME} data show a temperature increase of ca. 5-8 °C (using the BayMBT calibration; Martinez-Sosa et al., 2021) compared to the glacial stages immediately preceding and following. However, MIS 29, 27 and 21 were as warm or warmer than MIS 31 the MBT'_{5ME} record, yet Facies C is absent. This suggests that another factor besides temperature is responsible for, or contributes to, the formation of Facies C. The pollen record indicates that cool conifer forest was present around Lake El'gygytyn during MIS 31 and that higher precipitation characterized this superinterglacial (Zhao et al., 2018; Lozhkin and Anderson, 2013; Melles et al., 2012). Furthermore, based on mineral characteristics, Wei et al. (2014) demonstrated that precipitation is a key driver of Facies C. This may imply that MIS 29, 27, and 21 were relatively arid in comparison to MIS 31. Additionally, it is possible that MIS 31 was windier than other interglacials, thereby decreasing water column stability and increasing ventilation and nutrient availability in the surface waters. Indeed, high Si/Ti values, a proxy for diatom productivity, are noted in the Lake El'gygytyn record during MIS 31 (Melles et al., 2012).

420

In the interval from MIS 34 to 26, the *n*-alkane ACL record has the highest resolution during MIS 31. At this time, a shift to lower ACL values is noted (Fig. 2 and 5), potentially driven by wetter conditions. During the other interglacials in this interval (MIS 33, 29, and 27), lower ACL values generally occur during peak interglacial conditions. However, low sample resolution during MIS 27 hampers full evaluation of this relationship and higher variability in ACL values is noted during MIS 33, 29 and 27 compared to MIS 31. In the pollen record, MIS 29 is characterized by *Alnus* and *Betula* pollen while MIS 27 is characterized by an increase in larch, dwarf birch and alder pollen (Zhao et al., 2018). Our MBT'_{5ME} record differs from the pollen record in that MIS 29 appears warmer compared to MIS 27 whereas in the pollen record, MIS 27 is interpreted as the warmer and wetter of these interglacials (Zhao et al., 2018). The Lake El'gygytyn pollen record displays a sharp increase in cold steppe pollen at ~975 ka indicating the onset of glacial MIS 26 (Zhao et al., 2018). This dramatic change appears to be reflected in the ACL record with the largest shift in our record initiating at ~963 ka, when ACL values increase significantly (Fig. 2).

430

5.3.2 MIS 25-22 (959-866 ka)

In the Lake El'gygytyn brGDGT record, MIS 25 is comparatively cooler than other interglacial periods (Fig. 3). Summer insolation during MIS 25 reaches its highest value of the study interval yet reconstructed temperatures are similar to the preceding and following glacial stages when insolation and obliquity were lower. MBT'_{5ME} values average ~0.25, or 6°C on the BayMBT calibration. A relatively cool MIS 25 agrees with marine records, such as in the nearby Bering Sea where drastic

435



declines in both sea ice biomarkers and diatom productivity point to sea ice maxima during MIS 25 (Fig. 6g; Detlef et al., 2018), and in the North Pacific SST at ODP site 882 where low temperatures are recorded (Martínez-García et al., 2010). Following a brief increase in *n*-alkane ACL values at the termination of MIS 26, ACL again decline during the MIS 25 obliquity maximum circa 953 ka, indicating expansion of trees and shrubs, which is also noted in the pollen record (Zhao et al., 2018). Whereas Zhao et al. (2018) infer warm and moist conditions during MIS 25, the cool brGDGT-inferred temperatures suggest that the vegetation change was rather driven by a combination of longer growing seasons and increase in the moisture balance. Likewise, the Si/Ti ratio is slightly elevated during this interglacial (Fig. 3), suggesting an increase in lake productivity despite relatively cool summer temperatures.

Numerous MPT studies note a global cooling trend with increasing sea ice extent culminating in an anonymously cool or “skipped” MIS 23 interglacial and a strong glacial period during MIS 22 (Head & Gibbard, 2015 and references therein), in effect giving rise to the first long glacial cycle of the late-Pleistocene. The lack of warming at El’gygytyn during MIS 25 obscures the nature of the first long glacial cycle from MIS 24-22 that is apparent in the $\delta^{18}\text{O}$ history (Lisiecki and Raymo, 2005; Clark et al., 2006). From MIS 24 to 22, there is a strengthening of sub-orbital temperature variations, with two short lived warming excursions bracketing a brief cold period at 905 ka despite peaks in both obliquity and northern hemisphere summer insolation (Fig. 3). The evolutionary power spectrum shows that the strength of the 41-kyr climate variability weakens from MIS 25-22 whereas the sub-Milankovitch frequencies become more prominent (Fig. 4), suggesting a breakdown of the climate dynamics that dominated previously. The lower resolution ACL data are in closer agreement with the benthic isotope stack, exhibiting an increasing trend from MIS 25 to 22 and an abrupt decrease at the beginning of MIS 21 (Fig. 3).

Overprinting the increase in ACL values are a series of glacial-interglacial oscillations. For reasons that are not clear, pollen is absent in Lake El’gygytyn sediments during MIS 23 (Zhao et al., 2018) yet *n*-alkanes are present. During the peak of MIS 23, ACL values are high, and are higher than those of the previous glacials, suggesting conditions that were either arid or more glacial-like (Fig. 2). Temperatures during MIS 22 were particularly cold and arid, characterized by some of the lowest $\text{MBT}'_{5\text{ME}}$ values and ACL values of the record (Fig. 3). These cool conditions were associated with particularly low productivity, seen in the Si/Ti ratio (Fig. 3). There was a two-phase termination of MIS 22, with an abrupt warming at 880 ka followed by a brief return to cold conditions just prior to the final warming event. The two-phase deglaciation is also apparent in the doublet of Facies A during MIS 22 (Fig. 3). The deglacial warming is approximately synchronous with the increasing obliquity, leading the deglacial decrease in $\delta^{18}\text{O}$ (Fig. 3).

5.3.3 MIS 21-20 (866-790 ka)

While MIS 29, 27, and 21 all show $\text{MBT}'_{5\text{ME}}$ values as high as the superinterglacial MIS 31, the most pronounced warm period of the brGDGT record is MIS 21 (Fig. 3). Warming in the $\text{MBT}'_{5\text{ME}}$ starts early in MIS 22 and continues to ~868 ka when peak interglacial conditions are noted. Temperatures increased by at least 4 °C and possibly up to 10 °C at the start of MIS 21 as



470 seen in the BayMBT calibration. The comparatively rapid warming recorded at Lake El'gygytyn from MIS 22 to MIS 21,
agrees with Pacific records (Fig. 6; Martínez-Garcia et al., 2010; McClymont et al., 2013; Kender et al., 2018; Lattaud et al.,
2019). From 865-845 ka shrubby vegetation communities, including stone pine, birch and alder, returned to the region, while
n-alkane ACL decreased, thereby suggesting warm and wet conditions (Zhao et al., 2018). The reemergence of tree and shrub
communities during MIS 21 is also reflected in the loess sediments of northeast China (not shown; Zhou et al., 2018) suggesting
475 a widespread shift to milder conditions. Despite the notable warmth and a slight increase in aquatic productivity seen in the
Si/Ti ratios, MIS 21 is not identified as a superinterglacial interval based on the Si/Ti or lithofacies records (Melles et al.,
2012).

Interglacial conditions remained relatively warm for approximately 40 kyr during MIS 21-20. The return to glacial conditions
480 at El'gygytyn differs notably from the global benthic isotope composite (Lisiecki and Raymo, 2005); whereas the $\delta^{18}\text{O}$ data
indicate a gradual cooling or gradual development of ice sheets culminating in full glacial conditions around 814 ka, the
brGDGT data indicate an earlier and more rapid cooling to glacial conditions around 835 ka, which was then followed by
relatively stable or even warming climate moving into MIS 20 (Fig. 3). This early cooling is also seen in the pollen record,
which shows the appearance of open steppe vegetation from 845-810 ka (Zhao et al., 2018). The apparently cool, open-
485 landscape environment in the latter half of MIS 21 occurred despite increasing obliquity, reminiscent of the scenario across
MIS 25.

5.4 Comparison with North Pacific Marine Records

At present, air temperature anomalies at Lake El'gygytyn are largely governed by variations in the air masses originating
over the sub-Arctic North Pacific, the Bering Sea, and the proximal Arctic Ocean (Nolan and Brigham-Grette, 2007). Based
490 on this, Melles et al. (2012) hypothesized that temperatures during past interglacials were responsive to changes taking place
in the North Pacific Ocean. Specifically, the extremely warm and wet superinterglacials at El'gygytyn were linked to greater
stratification and hence higher SSTs in the North Pacific. The increased stratification in turn was hypothesized to be controlled
by southern hemisphere processes, namely reduced Antarctic Bottom Water flow into the Pacific basin. Since that study,
several new marine SST and upwelling records spanning the MPT have been developed from the North Pacific allowing for a
495 more direct assessment of this proposed mechanism.

The MPT temperature history at El'gygytyn generally resembles marine conditions at glacial-interglacial timescales (Fig. 6).
Biomarker records of sea ice expansion at Site U1343 (Fig. 6f) in the Bering Sea (Detlef et al., 2018) correspond to cool glacial
stages in the brGDGT record. Likewise, the reconstructed warmth and rapid onset of MIS 21 are also seen in SST records from
500 the Sea of Okhotsk (Lattaud et al., 2019) and ODP Site 882 (Martínez-Garcia et al., 2010), while cool conditions during MIS
25 are seen at both El'gygytyn and at Site 882 (Fig. 6b, d). However, the relationship with North Pacific upwelling appears
more complex. The strength of upwelling in the Bering Sea during the MPT was reconstructed using biogenic silica



505 accumulation rates and $\delta^{15}\text{N}$ offsets between Site U1343 in the Bering Sea and Site 1012 in the tropical North Pacific (Worne et al., 2020). During MIS 25, the cool temperatures recorded at El'gygytyn (Fig. 6b) and Site 882 (Fig. 6d) are consistent with a temporary increase in the upwelling index at Site U1343 (Fig. 6e). In contrast, during MIS 31, strengthened upwelling in the Bering corresponds with warm SST at Site 882 and superinterglacial conditions at El'gygytyn. The rapid transition into the notably warm MIS 21 coincides with warming seen in the nearby marine records (Martínez-García et al., 2010; Lattaud et al., 2019), and is likewise associated with an increase in Bering Sea upwelling (Fig. 6e; Worne et al., 2020).

510 A secular decline in upwelling at Site U1343 from MIS 30 to 22 corresponds with declining SSTs and expanding sea ice (Fig. 6e, f). These findings challenge the previous hypothesis of Melles et al. (2012) who suggested that reduced upwelling should cause an increase in temperature in the North Pacific and at El'gygytyn. To explain this, Worne et al. (2020) suggest that North Pacific cooling and sea ice expansion contributed to a reduction in upwelling via enhanced brine rejection on the Bering shelf and associated expansion of North Pacific Intermediate Waters. Worne et al. (2020) further hypothesize that the reduced upwelling suppresses CO_2 transfer from the deep Pacific to the atmosphere, providing an essential feedback to the global climate during MPT. This process was possibly enhanced by sea level decline (Berends et al., 2021; Elderfield et al., 2012) and the initial closure of the Bering Strait during MIS 23 (Kender et al., 2018). This mechanism is supported by North Pacific upwelling and surface water pH changes during the last glacial termination (Gray et al., 2018; Basak et al., 2018). The Lake El'gygytyn temperatures exhibit no strong trend associated with the decline in North Pacific upwelling. Rather, temperatures fluctuated, with minima occurring during both MIS 23, the first "skipped interglacial", and again during MIS 22 (Fig. 3 and 6). The high-frequency variability during MIS 23-21 approximates the half-precession timescales, potentially indicating a strengthening of tropical influences on the high latitudes during this critical transition period of the MPT.

525 While reduced upwelling did not drive a persistent increase or decrease in temperatures at Lake El'gygytyn across MIS 30-22, increased *n*-alkane ACL values, especially from MIS 26-22, suggest the continental climate was responsive to changes in the North Pacific (Fig. 6g). Vegetation assemblages at Lake El'gygytyn suggests a progression of arid, open steppe communities (Zhao et al., 2018). Increased sea ice coverage leading up to and during the 900 kyr event at MIS 23 (Fig. 6f) could have suppressed moisture transport to Lake El'gygytyn. Based on estimates of global sea levels during the MPT, Kender et al. (2018) suggest that the Bering Strait was open during both interglacial and glacial periods prior to MIS 24 then open only during interglacials afterwards. It remains unclear whether changes in sea ice volume and North Pacific circulation around MIS 26 prior to the Bering Strait closure were sufficient to suppress moisture transport at Lake El'gygytyn or if the Bering Strait might have closed during that glacial. High-resolution sea ice reconstructions from the Arctic Ocean are needed to better evaluate moisture source changes across the MPT.



6. Conclusions

535 The Lake El'gygytgyn brGDGT reconstruction presented here is the only time-continuous record of Arctic continental
temperatures spanning the MPT, thereby providing novel insights into the role and the response of high-latitude climate
through the mid-Pleistocene. Our new brGDGT record of relative temperature variability captures glacial-interglacial climate
540 fluctuations at Lake El'gygytgyn although the ability of brGDGTs to reconstruct absolute temperature is less clear and a pan-
Arctic or site-specific calibration may be needed. The finding that variability expressed in the brGDGT temperature record,
together with comparison to marine records, suggests that obliquity, precession, and possibly half-precession are persistent
characteristics of high-latitude climate across the MPT. While some locations indicate an overall cooling trend throughout the
MPT, this is not observed at Lake El'gygytgyn. We find that MIS 31, which is widely recognized as a particularly warm
interglacial, does not exhibit exceptional warmth in the brGDGT record but instead find that MIS 21 was an especially warm
interglacial both at Lake El'gygytgyn and throughout much of the North Pacific region. Throughout the MPT, Lake El'gygytgyn
545 pollen and *n*-alkane data exhibit a long-term cooling and drying trend, with a shift to an increasingly open landscape noted
after around 900 ka (Zhao et al., 2018). The lack of overall MPT cooling in our terrestrial record contradicts upwelling-driven
climate trends observed in North Pacific marine proxies. Having a better understanding of history of the Bering Strait's closure
will be critical for resolving the differences between terrestrial and marine climate records in the region. Our new data from
Lake El'gygytgyn provide a number of constraints for understanding the evolution of Arctic temperature change across the
550 mid-Pleistocene.

7. Data Availability

The biomarker (*n*-alkane and GDGT) data used in this study is archived at the NOAA National Centers for Environmental
Information: <https://www.ncdc.noaa.gov/paleo/study/33552>

8. Acknowledgements

555 This work was supported by the National Science Foundation (grant number 1204087) and a University of Massachusetts
Amherst Commonwealth Honors College undergraduate research grant awarded to Kurt Lindberg. We thank Martin Melles,
Volker Wennrich, and numerous other international collaborators of the Lake El'gygytgyn Drilling Project. We also thank
Anders Noren, Kristina Brady and the staff at LacCore for their assistance and support with numerous large sample requests,
as well as John Sweeney and Jeff Salacup at University of Massachusetts for technical support.



560 9. Supplement

The supplement to this manuscript is uploaded for review along with the main text. This statement will be revised once a DOI is assigned.

References

- Andersson, R. A., Kuhry, P., Meyers, P., Zebühr, Y., Crill, P., and Mörth, M.: Impacts of paleohydrological changes on n-alkane biomarker compositions of a Holocene peat sequence in the eastern European Russian Arctic, *Organic Geochemistry*, 42, 1065-1075, 2011.
- Basak, C., Fröllje, H., Lamy, F., Gersonde, R., Benz, V., Anderson, R. F., Molina-Kescher, M., and Pahnke, K.: Breakup of last glacial deep stratification in the South Pacific, *Science*, 359, 900-904, 2018.
- Berends, C. J., de Boer, B., and van de Wal, R. S.: Reconstructing the evolution of ice sheets, sea level, and atmospheric CO₂ during the past 3.6 million years, *Climate of the Past*, 17, 361-377, 2021.
- 570 Berger, A., and Loutre, M.-F.: Insolation values for the climate of the last 10 million years, *Quaternary Science Reviews*, 10, 297-317, 1991.
- Billups, K., York, K., and Bradtmiller, L. I.: Water column stratification in the Antarctic zone of the Southern Ocean during the mid-Pleistocene climate transition, *Paleoceanography and Paleoclimatology*, 33, 432-442, 2018.
- Bray, E., and Evans, E.: Distribution of n-paraffins as a clue to recognition of source beds, *Geochimica et Cosmochimica Acta*, 22, 2-15, 1961.
- 575 Brigham-Grette, J., Melles, M., and Minyuk, P.: Overview and significance of a 250 ka paleoclimate record from El'gygytyn Crater Lake, NE Russia, *Journal of Paleolimnology*, 37, 1-16, 2007.
- Brigham-Grette, J., Melles, M., Minyuk, P., Andreev, A., Tarasov, P., DeConto, R., Koenig, S., Nowaczyk, N., Wennrich, V., and Rosén, P.: Pliocene warmth, polar amplification, and stepped Pleistocene cooling recorded in NE Arctic Russia, *Science*, 340, 1421-1427, 2013.
- Bush, R. T., and McInerney, F. A.: Leaf wax n-alkane distributions in and across modern plants: implications for paleoecology and chemotaxonomy, *Geochimica et Cosmochimica Acta*, 117, 161-179, 2013.
- 580 Bush, R. T., and McInerney, F. A.: Influence of temperature and C₄ abundance on n-alkane chain length distributions across the central USA, *Organic Geochemistry*, 79, 65-73, 2015.
- Castañeda, I. S., Werne, J. P., Johnson, T. C., and Filley, T. R.: Late Quaternary vegetation history of southeast Africa: the molecular isotopic record from Lake Malawi, *Palaeogeography, Palaeoclimatology, Palaeoecology*, 275, 100-112, 2009.
- 585 Castañeda, I. S., and Schouten, S.: A review of molecular organic proxies for examining modern and ancient lacustrine environments, *Quaternary Science Reviews*, 30, 2851-2891, 2011.
- Clark, P. U., and Pollard, D.: Origin of the middle Pleistocene transition by ice sheet erosion of regolith, *Paleoceanography*, 13, 1-9, 1998.
- Clark, P. U., Archer, D., Pollard, D., Blum, J. D., Rial, J. A., Brovkin, V., Mix, A. C., Pisias, N. G., and Roy, M.: The middle Pleistocene transition: characteristics, mechanisms, and implications for long-term changes in atmospheric pCO₂, *Quaternary Science Reviews*, 25, 3150-3184, 2006.
- 590 Cremer, H., Wagner, B., Juschus, O., and Melles, M.: A microscopical study of diatom phytoplankton in deep crater Lake El'gygytyn, Northeast Siberia, *Algological Studies*, 116, 147-169, 2005.
- D'Anjou, R., Wei, J., Castañeda, I., Brigham-Grette, J., Petsch, S., and Finkelstein, D.: High-latitude environmental change during MIS 9 and 11: biogeochemical evidence from Lake El'gygytyn, Far East Russia, *Climate of the Past*, 9, 567-581, 2013.
- 595 Da, J., Zhang, Y. G., Li, G., Meng, X., and Ji, J.: Low CO₂ levels of the entire Pleistocene epoch, *Nature communications*, 10, 1-9, 2019.
- Dang, X., Ding, W., Yang, H., Pancost, R. D., Naafs, B. D. A., Xue, J., Lin, X., Lu, J., and Xie, S.: Different temperature dependence of the bacterial brGDGT isomers in 35 Chinese lake sediments compared to that in soils, *Organic Geochemistry*, 119, 72-79, 2018.
- Daniels, W., Castañeda, I., Salacup, J. M., Habicht, M. H., Lindberg, K., and Brigham-Grette, J.: Archaeal lipids reveal climate-driven changes in microbial ecology at Lake El'gygytyn (Far East Russia) during the Plio-Pleistocene, *Journal of Quaternary Science*, in review.
- 600 Daniels, W. C., Russell, J. M., Giblin, A. E., Welker, J. M., Klein, E. S., and Huang, Y.: Hydrogen isotope fractionation in leaf waxes in the Alaskan Arctic tundra, *Geochimica et Cosmochimica Acta*, 213, 216-236, 2017.
- Davy, R., Chen, L., and Hanna, E.: Arctic amplification metrics, *International Journal of Climatology*, 38, 4384-4394, 2018.
- De Jonge, C., Hopmans, E. C., Zell, C. I., Kim, J.-H., Schouten, S., and Sinninghe Damsté, J. S.: Occurrence and abundance of 6-methyl branched glycerol dialkyl glycerol tetraethers in soils: Implications for palaeoclimate reconstruction, *Geochimica et Cosmochimica Acta*, 141, 97-112, 2014.
- 605 de Wet, G. A., Castañeda, I. S., DeConto, R. M., and Brigham-Grette, J.: A high-resolution mid-Pleistocene temperature record from Arctic Lake El'gygytyn: a 50 kyr super interglacial from MIS 33 to MIS 31?, *Earth and Planetary Science Letters*, 436, 56-63, 10.1016/j.epsl.2015.12.021, 2016.
- de Wet, G. A.: Arctic and North Atlantic paleo-environmental reconstructions from lake sediments, 2017.



- 610 Detlef, H., Belt, S., Sosdian, S., Smik, L., Lear, C., Hall, I., Cabedo-Sanz, P., Husum, K., and Kender, S.: Sea ice dynamics across the Mid-Pleistocene transition in the Bering Sea, *Nature communications*, 9, 1-11, 2018.
Dipre, G. R., Polyak, L., Kuznetsov, A. B., Oti, E. A., Ortiz, J. D., Brachfeld, S. A., Xuan, C., Lazar, K. B., and Cook, A. E.: Plio-Pleistocene sedimentary record from the Northwind Ridge: new insights into paleoclimatic evolution of the western Arctic Ocean for the last 5 Ma, *arktos*, 4, 1-23, 2018.
- 615 Eglinton, G., and Hamilton, R. J.: Leaf epicuticular waxes, *Science*, 156, 1322-1335, 1967.
Elderfield, H., Ferretti, P., Greaves, M., Crowhurst, S., McCave, I. N., Hodell, D., and Piotrowski, A. M.: Evolution of ocean temperature and ice volume through the mid-Pleistocene climate transition, *science*, 337, 704-709, 2012.
Ferretti, P., Crowhurst, S. J., Hall, M. A., and Cacho, I.: North Atlantic millennial-scale climate variability 910 to 790 ka and the role of the equatorial insolation forcing, *Earth and Planetary Science Letters*, 293, 28-41, 2010.
- 620 Ford, H. L., and Raymo, M. E.: Regional and global signals in seawater $\delta^{18}O$ records across the mid-Pleistocene transition, *Geology*, 48, 113-117, 2020.
Francke, A., Wennrich, V., Sauerbrey, M., Juschus, O., Melles, M., and Brigham-Grette, J.: Multivariate statistic and time series analyses of grain-size data in quaternary sediments of Lake El'gygytyn, NE Russia, *Climate of the Past*, 9, 2459-2470, 2013.
Gagosian, R. B., and Peltzer, E. T.: The importance of atmospheric input of terrestrial organic material to deep sea sediments, *Organic Geochemistry*, 10, 661-669, 1986.
- 625 Gray, W. R., Rae, J. W., Wills, R. C., Shevenell, A. E., Taylor, B., Burke, A., Foster, G. L., and Lear, C. H.: Deglacial upwelling, productivity and CO₂ outgassing in the North Pacific Ocean, *Nature Geoscience*, 11, 340-344, 2018.
Hammer, Ø., Harper, D. A., and Ryan, P. D.: PAST: Paleontological statistics software package for education and data analysis, *Palaeontologia electronica*, 4, 9, 2001.
- 630 Han, W., Fang, X., and Berger, A.: Tibet forcing of mid-Pleistocene synchronous enhancement of East Asian winter and summer monsoons revealed by Chinese loess record, *Quaternary Research*, 78, 174-184, 2012.
Haneda, Y., Okada, M., Kubota, Y., and Suganuma, Y.: Millennial-scale hydrographic changes in the northwestern Pacific during marine isotope stage 19: teleconnections with ice melt in the North Atlantic, *Earth and Planetary Science Letters*, 531, 115936, 2020.
Hasenfratz, A. P., Jaccard, S. L., Martínez-García, A., Sigman, D. M., Hodell, D. A., Vance, D., Bernasconi, S. M., Kleiven, H. K. F.,
635 Haumann, F. A., and Haug, G. H.: The residence time of Southern Ocean surface waters and the 100,000-year ice age cycle, *Science*, 363, 1080-1084, 2019.
Heslop, D., Dekkers, M., and Langereis, C.: Timing and structure of the mid-Pleistocene transition: records from the loess deposits of northern China, *Palaeogeography, Palaeoclimatology, Palaeoecology*, 185, 133-143, 2002.
- 640 Holland, A., Petsch, S., Castaneda, I., Wilkie, K., Burns, S., and Brigham-Grette, J.: A biomarker record of Lake El'gygytyn, Far East Russian Arctic: investigating sources of organic matter and carbon cycling during marine isotope stages 1-3, *Climate of the Past*, 9, 243-260, 2013.
Hönisch, B., Hemming, N. G., Archer, D., Siddall, M., and McManus, J. F.: Atmospheric carbon dioxide concentration across the mid-Pleistocene transition, *Science*, 324, 1551-1554, 2009.
Hopmans, E. C., Schouten, S., and Sinninghe Damsté, J. S.: The effect of improved chromatography on GDGT-based palaeoproxies, *Organic Geochemistry*, 93, 1-6, 2016.
- 645 Hugué, C., Hopmans, E. C., Febo-Ayala, W., Thompson, D. H., Damsté, J. S. S., and Schouten, S.: An improved method to determine the absolute abundance of glycerol dibiphytanyl glycerol tetraether lipids, *Organic Geochemistry*, 37, 1036-1041, 2006.
Huybers, P., and Wunsch, C.: Obliquity pacing of the late Pleistocene glacial terminations, *Nature*, 434, 491-494, 2005.
Kawamura, K., Ishimura, Y., and Yamazaki, K.: Four years' observations of terrestrial lipid class compounds in marine aerosols from the western North Pacific, *Global Biogeochemical Cycles*, 17, 3-1-3-19, 2003.
- 650 Keisling, B. A., Castañeda, I. S., and Brigham-Grette, J.: Hydrological and temperature change in Arctic Siberia during the intensification of Northern Hemisphere Glaciation, *Earth and Planetary Science Letters*, 457, 136-148, 2017.
Kender, S., Ravelo, A. C., Worne, S., Swann, G. E., Leng, M. J., Asahi, H., Becker, J., Detlef, H., Aiello, I. W., and Andreasen, D.: Closure of the Bering Strait caused mid-Pleistocene transition cooling, *Nature communications*, 9, 1-11, 2018.
- 655 Laskar, J., Robutel, P., Joutel, F., Gastineau, M., Correia, A., and Levrard, B.: A long-term numerical solution for the insolation quantities of the Earth, *Astronomy & Astrophysics*, 428, 261-285, 2004.
Lattaud, J., Lo, L., Huang, J. J., Chou, Y. M., Gorbarenko, S. A., Sinninghe Damsté, J. S., and Schouten, S.: A Comparison of Late Quaternary Organic Proxy-Based Paleotemperature Records of the Central Sea of Okhotsk, *Paleoceanography and paleoclimatology*, 33, 732-744, 2018.
Lattaud, J., Lo, L., Zeeden, C., Liu, Y.-J., Song, S.-R., Van Der Meer, M. T., Damsté, J. S. S., and Schouten, S.: A multiproxy study of past environmental changes in the Sea of Okhotsk during the last 1.5 Ma, *Organic Geochemistry*, 132, 50-61, 2019.
- 660 Lawrence, K. T., Herbert, T. D., Brown, C. M., Raymo, M. E., and Haywood, A. M.: High-amplitude variations in North Atlantic sea surface temperature during the early Pliocene warm period, *Paleoceanography*, 24, 2009.
Layer, P. W.: Argon-40/argon-39 age of the El'gygytyn impact event, Chukotka, Russia, *Meteoritics & Planetary Science*, 35, 591-599, 2000.



- 665 Li, B., Wang, J., Huang, B., Li, Q., Jian, Z., Zhao, Q., Su, X., and Wang, P.: South China Sea surface water evolution over the last 12 Myr: A south-north comparison from Ocean Drilling Program Sites 1143 and 1146, *Paleoceanography*, 19, 2004.
- Lisiecki, L. E., and Raymo, M. E.: A Pliocene-Pleistocene stack of 57 globally distributed benthic $\delta^{18}\text{O}$ records, *Paleoceanography*, 20, 2005.
- 670 Liu, W., and Huang, Y.: Compound specific D/H ratios and molecular distributions of higher plant leaf waxes as novel paleoenvironmental indicators in the Chinese Loess Plateau, *Organic geochemistry*, 36, 851-860, 2005.
- Lomb, N. R.: Least-squares frequency analysis of unequally spaced data, *Astrophysics and space science*, 39, 447-462, 1976.
- Lozhkin, A., and Anderson, P.: Vegetation responses to interglacial warming in the Arctic: examples from Lake El'gygytgyn, Far East Russian Arctic, *Climate of the Past*, 9, 1211-1219, 2013.
- 675 Maiorano, P., Marino, M., and Flores, J.-A.: The warm interglacial Marine Isotope Stage 31: Evidences from the calcareous nannofossil assemblages at Site 1090 (Southern Ocean), *Marine Micropaleontology*, 71, 166-175, 2009.
- Martínez-García, A., Rosell-Melé, A., McClymont, E. L., Gersonde, R., and Haug, G. H.: Subpolar link to the emergence of the modern equatorial Pacific cold tongue, *Science*, 328, 1550-1553, 2010.
- Martínez-Sosa, P., Tierney, J., Stefanescu, I. C., Crampton-Flood, E. D., Shuman, B. N., and Routsom, C.: A global Bayesian temperature calibration for lacustrine brGDGTs, 2021.
- 680 McClymont, E. L., Rosell-Melé, A., Haug, G. H., and Lloyd, J. M.: Expansion of subarctic water masses in the North Atlantic and Pacific oceans and implications for mid-Pleistocene ice sheet growth, *Paleoceanography*, 23, 2008.
- McClymont, E. L., Sosdian, S. M., Rosell-Melé, A., and Rosenthal, Y.: Pleistocene sea-surface temperature evolution: Early cooling, delayed glacial intensification, and implications for the mid-Pleistocene climate transition, *Earth-Science Reviews*, 123, 173-193, 2013.
- Melles, M., Brigham-Grette, J., Minyuk, P. S., Nowaczyk, N. R., Wennrich, V., DeConto, R. M., Anderson, P. M., Andreev, A. A., Coletti, A., and Cook, T. L.: 2.8 million years of Arctic climate change from Lake El'gygytgyn, NE Russia, *Science*, 337, 315-320, 2012.
- 685 Meyers, P. A.: Applications of organic geochemistry to paleolimnological reconstructions: a summary of examples from the Laurentian Great Lakes, *Organic geochemistry*, 34, 261-289, 2003.
- Miller, D. R., Habicht, M. H., Keisling, B. A., Castañeda, I. S., and Bradley, R. S.: A 900-year New England temperature reconstruction from in situ seasonally produced branched glycerol dialkyl glycerol tetraethers (brGDGTs), *Climate of the Past*, 14, 1653-1667, 2018.
- 690 Miller, G. H., Brigham-Grette, J., Alley, R., Anderson, L., Bauch, H. A., Douglas, M., Edwards, M., Elias, S., Finney, B., and Fitzpatrick, J. J.: Temperature and precipitation history of the Arctic, *Quaternary Science Reviews*, 29, 1679-1715, 2010.
- Müller, J., Romero, O., Cowan, E. A., McClymont, E. L., Forwick, M., Asahi, H., März, C., Moy, C. M., Suto, I., and Mix, A.: Cordilleran ice-sheet growth fueled primary productivity in the Gulf of Alaska, northeast Pacific Ocean, *Geology*, 46, 307-310, 2018.
- Nolan, M., and Brigham-Grette, J.: Basic hydrology, limnology, and meteorology of modern Lake El'gygytgyn, Siberia, *Journal of Paleolimnology*, 37, 17-35, 2007.
- 695 Nolan, M., Cassano, E., and Cassano, J.: Synoptic climatology and recent climate trends at Lake El'gygytgyn, *Climate of the Past*, 9, 1271-1286, 2013.
- Nowaczyk, N. R., Haltia, E., Ulbricht, D., Wennrich, V., Sauerbrey, M., Rosén, P., Vogel, H., Francke, A., Meyer-Jacob, C., and Andreev, A.: Chronology of Lake El'gygytgyn sediments—a combined magnetostratigraphic, palaeoclimatic and orbital tuning study based on multi-parameter analyses, *Climate of the Past*, 9, 2413-2432, 2013.
- 700 O'Connor, K. F., Berke, M. A., and Ziolkowski, L. A.: Hydrogen isotope fractionation in modern plants along a boreal-tundra transect in Alaska, *Organic Geochemistry*, 147, 104064, 2020.
- Paillard, D.: The timing of Pleistocene glaciations from a simple multiple-state climate model, *Nature*, 391, 378-381, 1998.
- Past Interglacial Working Group of PAGES: Interglacials of the last 800,000 years, *Reviews of Geophysics*, 54, 162-219, 2016.
- 705 Pearson, E. J., Juggins, S., Talbot, H. M., Weckström, J., Rosén, P., Ryves, D. B., Roberts, S. J., and Schmidt, R.: A lacustrine GDGT-temperature calibration from the Scandinavian Arctic to Antarctic: Renewed potential for the application of GDGT-paleothermometry in lakes, *Geochimica et Cosmochimica Acta*, 75, 6225-6238, 2011.
- Peltzer, E.: Organic geochemistry of aerosols over the Pacific Ocean, *Chemical oceanography*, 10, 281-338, 1989.
- 710 Pena, L. D., and Goldstein, S. L.: Thermohaline circulation crisis and impacts during the mid-Pleistocene transition, *Science*, 345, 318-322, 2014.
- Peterse, F., Vonk, J. E., Holmes, R. M., Giosan, L., Zimov, N., and Eglinton, T. I.: Branched glycerol dialkyl glycerol tetraethers in Arctic lake sediments: Sources and implications for paleothermometry at high latitudes, *Journal of Geophysical Research: Biogeosciences*, 119, 1738-1754, 2014.
- Poirier, R. K., and Billups, K.: The intensification of northern component deepwater formation during the mid-Pleistocene climate transition, *Paleoceanography*, 29, 1046-1061, 2014.
- 715 Pollard, D., and DeConto, R. M.: Modelling West Antarctic ice sheet growth and collapse through the past five million years, *Nature*, 458, 329-332, 2009.
- Poynter, J., Farrimond, P., Robinson, N., and Eglinton, G.: Aeolian-derived higher plant lipids in the marine sedimentary record: Links with palaeoclimate, in: *Paleoclimatology and paleometeorology: modern and past patterns of global atmospheric transport*, Springer, 435-462, 1989.
- 720



- Raberg, J. H., Harning, D. J., Crump, S. E., de Wet, G., Blumm, A., Kopf, S., Geirsdóttir, Á., Miller, G. H., and Sepúlveda, J.: Revised fractional abundances and warm-season temperatures substantially improve brGDGT calibrations in lake sediments, *Biogeosciences Discussions*, 1-36, 2021.
- Raymo, M.: The timing of major climate terminations, *Paleoceanography*, 12, 577-585, 1997.
- 725 Rodríguez-Sanz, L., Mortyn, P. G., Martínez-García, A., Rosell-Melé, A., and Hall, I. R.: Glacial Southern Ocean freshening at the onset of the middle Pleistocene climate transition, *Earth and Planetary Science Letters*, 345, 194-202, 2012.
- Rommerskirchen, F., Eglinton, G., Dupont, L., Güntner, U., Wenzel, C., and Rullkötter, J.: A north to south transect of Holocene southeast Atlantic continental margin sediments: Relationship between aerosol transport and compound-specific $\delta^{13}\text{C}$ land plant biomarker and pollen records, *Geochemistry, Geophysics, Geosystems*, 4, 2003.
- 730 Roy, M., Clark, P. U., Raisbeck, G. M., and Yiou, F.: Geochemical constraints on the regolith hypothesis for the middle Pleistocene transition, *Earth and Planetary Science Letters*, 227, 281-296, 2004.
- Russell, J. M., Hopmans, E. C., Loomis, S. E., Liang, J., and Sinninghe Damsté, J. S.: Distributions of 5- and 6-methyl branched glycerol dialkyl glycerol tetraethers (brGDGTs) in East African lake sediment: Effects of temperature, pH, and new lacustrine paleotemperature calibrations, *Organic Geochemistry*, 117, 56-69, 2018.
- 735 Saltzman, B., and Verbitsky, M. Y.: Multiple instabilities and modes of glacial rhythmicity in the Plio-Pleistocene: a general theory of late Cenozoic climatic change, *Climate Dynamics*, 9, 1-15, 1993.
- Scargle, J. D.: Studies in astronomical time series analysis. II-Statistical aspects of spectral analysis of unevenly spaced data, *The Astrophysical Journal*, 263, 835-853, 1982.
- Schefuß, E., Ratmeyer, V., Stuut, J.-B. W., Jansen, J. F., and Damsté, J. S. S.: Carbon isotope analyses of n-alkanes in dust from the lower atmosphere over the central eastern Atlantic, *Geochimica et Cosmochimica Acta*, 67, 1757-1767, 2003.
- 740 Schouten, S., Hopmans, E. C., Schefuß, E., and Sinninghe Damsté, J. S.: Distributional variations in marine crenarchaeotal membrane lipids: a new tool for reconstructing ancient sea water temperatures?, *Earth and Planetary Science Letters*, 204, 265-274, 2002.
- Schulz, M., and Mudelsee, M.: REDFIT: estimating red-noise spectra directly from unevenly spaced paleoclimatic time series, *Computers & Geosciences*, 28, 421-426, 2002.
- 745 Serreze, M., Barrett, A., Stroeve, J., Kindig, D., and Holland, M.: The emergence of surface-based Arctic amplification, *The Cryosphere*, 3, 11-19, 2009.
- Shanahan, T. M., Hughen, K. A., and Van Mooy, B. A.: Temperature sensitivity of branched and isoprenoid GDGTs in Arctic lakes, *Organic Geochemistry*, 64, 119-128, 2013.
- Sinninghe Damsté, J. S., Hopmans, E. C., Pancost, R. D., Schouten, S., and Geenevasen, J. A.: Newly discovered non-isoprenoid glycerol dialkyl glycerol tetraether lipids in sediments, *Chemical Communications*, 1683-1684, 2000.
- 750 Soudian, S., and Rosenthal, Y.: Deep-sea temperature and ice volume changes across the Pliocene-Pleistocene climate transitions, *Science*, 325, 306-310, 2009.
- Sun, Q., Chu, G., Liu, M., Xie, M., Li, S., Ling, Y., Wang, X., Shi, L., Jia, G., and Lü, H.: Distributions and temperature dependence of branched glycerol dialkyl glycerol tetraethers in recent lacustrine sediments from China and Nepal, *Journal of Geophysical Research: Biogeosciences*, 116, 2011.
- 755 Teitler, L., Florindo, F., Warnke, D. A., Filippelli, G. M., Kupp, G., and Taylor, B.: Antarctic Ice Sheet response to a long warm interval across Marine Isotope Stage 31: A cross-latitude study of iceberg-rafted debris, *Earth and Planetary Science Letters*, 409, 109-119, 2015.
- Thomas, E. K., Clemens, S. C., Sun, Y., Prell, W. L., Huang, Y., Gao, L., Loomis, S., Chen, G., and Liu, Z.: Heterodynes dominate precipitation isotopes in the East Asian monsoon region, reflecting interaction of multiple climate factors, *Earth and Planetary Science Letters*, 455, 196-206, 2016.
- 760 Thomas, E. K., Castañeda, I., McKay, N., Briner, J., Salacup, J., Nguyen, K., and Schweinsberg, A.: A wetter Arctic coincident with hemispheric warming 8,000 years ago, *Geophysical Research Letters*, 45, 10.637-610.647, 2018.
- Verschuren, D., Damsté, J. S. S., Moernaut, J., Kristen, I., Blaauw, M., Fagot, M., and Haug, G. H.: Half-precessional dynamics of monsoon rainfall near the East African Equator, *Nature*, 462, 637-641, 2009.
- 765 Wara, M., Ravelo, A., and Delaney, M.: Reconstruction of eastern and western tropical Pacific sea surface temperatures and oxygen isotopic composition of surface seawater, 5 Ma to present, AGU Fall Meeting Abstracts, 2002, PP62A-0330.
- Wei, J. H., Finkelstein, D. B., Brigham-Grette, J., Castañeda, I. S., and Nowaczyk, N.: Sediment colour reflectance spectroscopy as a proxy for wet/dry cycles at Lake El'gygytgyn, Far East Russia, during Marine Isotope Stages 8 to 12, *Sedimentology*, 61, 1793-1811, 2014.
- 770 Weijers, J. W., Schouten, S., van den Donker, J. C., Hopmans, E. C., and Sinninghe Damsté, J. S.: Environmental controls on bacterial tetraether membrane lipid distribution in soils, *Geochimica et Cosmochimica Acta*, 71, 703-713, 2007.
- Wennrich, V., Francke, A., Dehnert, A., Juschus, O., Leipe, T., Vogt, C., Brigham-Grette, J., Minyuk, P., and Melles, M.: Modern sedimentation patterns in Lake El'gygytgyn, NE Russia, derived from surface sediment and inlet streams samples, *Climate of the Past*, 9, 135-148, 2013.
- 775 Wennrich, V., Minyuk, P., Borkhodoev, V., Francke, A., Ritter, B., Nowaczyk, N. R., Sauerbrey, M., Brigham-Grette, J., and Melles, M.: Pliocene to Pleistocene climate and environmental history of Lake El'gygytgyn, Far East Russian Arctic, based on high-resolution inorganic geochemistry data, *Climate of the Past*, 10, 1381-1399, 2014.



- 780 Wilkie, K., Chaplignin, B., Meyer, H., Burns, S., Petsch, S., and Brigham-Grette, J.: Modern isotope hydrology and controls on δD of plant leaf waxes at Lake El'gygytgyn, NE Russia, *Climate of the Past*, 9, 335-352, 2013.
- Willeit, M., Ganopolski, A., Calov, R., and Brovkin, V.: Mid-Pleistocene transition in glacial cycles explained by declining CO₂ and regolith removal, *Science Advances*, 5, eaav7337, 2019.
- Worne, S., Kender, S., Swann, G. E., Leng, M. J., and Ravelo, A. C.: Reduced upwelling of nutrient and carbon-rich water in the subarctic Pacific during the Mid-Pleistocene Transition, *Palaeogeography, Palaeoclimatology, Palaeoecology*, 555, 109845, 2020.
- Wu, F., Fang, X., and Miao, Y.: Aridification history of the West Kunlun Mountains since the mid-Pleistocene based on sporopollen and microcharcoal records, *Palaeogeography, Palaeoclimatology, Palaeoecology*, 547, 109680, 2020.
- 785 Zhang, Z., Zhao, M., Eglinton, G., Lu, H., and Huang, C.-Y.: Leaf wax lipids as paleovegetational and paleoenvironmental proxies for the Chinese Loess Plateau over the last 170 kyr, *Quaternary Science Reviews*, 25, 575-594, 2006.
- Zhao, B., Castañeda, I. S., Bradley, R. S., Salacup, J. M., Daniels, W., Schneider, T., and de Wet, G.: Reconstructing summer water temperature from a southern Greenland lake over the Common Era: a site-specific calibration for brGDGTs, *AGU Fall Meeting 2020*, 2020, 2020.
- 790 Zhao, B., Castañeda, I. S., Bradley, R. S., Salacup, J. M., Gregory, A., Daniels, W. C., and Schneider, T.: Development of an in situ branched GDGT calibration in Lake 578, southern Greenland, *Organic Geochemistry*, 104168, 2021.
- Zhao, W., Tarasov, P. E., Lozhkin, A. V., Anderson, P. M., Andreev, A. A., Korzun, J. A., Melles, M., Nedorubova, E. Y., and Wennrich, V.: High-latitude vegetation and climate changes during the Mid-Pleistocene Transition inferred from a palynological record from Lake El'gygytgyn, NE Russian Arctic, *Boreas*, 47, 137-149, 2018.
- 795 Zhou, X., Yang, J., Wang, S., Xiao, G., Zhao, K., Zheng, Y., Shen, H., and Li, X.: Vegetation change and evolutionary response of large mammal fauna during the Mid-Pleistocene Transition in temperate northern East Asia, *Palaeogeography, Palaeoclimatology, Palaeoecology*, 505, 287-294, 2018.

800